Benchmarking photoactive thin-film materials using a laser-induced steady-state photocarrier grating

L.W. Veldhuizen[1*], G.W.P. Adhyaksa[2], M. Theelen[3], E.C. Garnett[2] and R.E.I. Schropp[1]

*Corresponding Author

[1]Eindhoven University of Technology (TU/e)

Department of Applied Physics, Plasma & Materials Processing

P.O. Box 513, 5600 MB Eindhoven, The Netherlands

e-mail: l.w.veldhuizen@tue.nl

[2]FOM Institute AMOLF

Center for Nanophotonics

Science Park 104, 1098 XG Amsterdam, The Netherlands

[3]TNO/Solliance, Thin Film Technology

High Tech Campus 21, 5656 AE Eindhoven, The Netherlands

Abstract

In this study we assess the charge carrier diffusive transport quality of traditional and emerging thin-film photoactive absorber materials used for photovoltaic applications. We characterize our films using a steady-state photocarrier grating technique that has so far primarily been used for amorphous silicon-based materials. This data is combined with steady-state photoconductivity measurements to obtain ambipolar diffusion lengths as well as minority and majority carrier mobility-lifetime products. We also analyze the optical quality of the materials by calculating an effective absorption depth for sunlight and compare its value to the ambipolar diffusion length. We observe that for silicon-based thin-film materials, the ambipolar diffusion length is much shorter than their effective absorption depth, while for the copper indium gallium selenide chalcopyrite and mixed halide perovskite materials the diffusion length is similar or larger than the effective absorption depth. The presented method can be used as a benchmark for the current harvesting capabilities of a wide variety of thin-film absorber materials.

From an optical point of view, one would prefer a photovoltaic absorber material to be as optically thick as possible in order to generate the highest possible photocurrent. From an electrical and often economical perspective however, one would desire the absorber to be made as thin as possible. The optimal layer thickness in this inevitable trade-off is to a significant extent governed by the electronic transport properties of photocarriers in the material. While built-in electric fields in photovoltaic devices can assist carrier transport by means of drift, all absorber materials rely at least partially on the diffusion of photocarriers for the collection of current. For this reason it is valuable to know the ambipolar diffusion length (L_d) of a photoactive material, which is defined as the average distance travelled by charge carriers under ambipolar transport conditions before recombining[1]. A sufficiently high value of L_d is important for achieving high efficiency of photovoltaic devices[2-4] and high current gains in bipolar transistors[5]. Because the ambipolar diffusion length is dominated by the minority carriers, i.e. the transport-limiting carriers, it cannot be obtained using steady-state photoconductivity measurements. Commonly, the minority carrier diffusion properties are accessed using methods such as time of flight[6] (ToF), time-resolved photoluminescence[7] (TRPL), time-resolved terahertz spectroscopy[8] (TRTS) or surface photovoltage[9,10] (SPV) measurements. Although these methods can be very powerful, they also have several limitations. The ToF, TRPL and TRTS methods are, for instance, transient measurements that are based on numerous assumptions, whereas SPV measurements require samples with a thin space charge region and a large thickness compared to L_d. A particularly elegant and swift alternative method is the steady-state photocarrier grating technique (SSPG) which can be performed under conditions that are close to the operating conditions of solar cells and using thin-film samples not requiring selective contacts characterized with only basic optical and electronic equipment. Since the method was established by Ritter, Zeldov and Weiser[11], it has been used predominantly for the characterization of thin-film silicon and related materials[12].

In this work we expand the use of the technique to modern photoactive thin film materials by measuring the lateral carrier diffusion properties of device quality copper indium gallium selenide chalcopyrite ($Cu(In,Ga)Se_2$) and two types of emerging hybrid organic-inorganic lead halide perovskite ($MAPbBr_3$ and $MAPbI_{3-x}Cl_x$) films. In addition to that, we characterize hydrogenated amorphous and microcrystalline silicon (a-Si:H, μc-Si:H) as well as hydrogenated silicon-germanium (a-SiGe:H) to obtain a reference base of the carrier diffusion properties of both traditional and emerging thin-film photoactive absorber materials, measured under the same conditions.

A fair comparison of the various carrier transport properties of this wide range of photoabsorber materials cannot be properly done without also considering the optical properties of the materials, since a weakly absorbing material requires both a larger thickness and larger diffusion length compared to a strongly absorbing material. Hence, in order to benchmark these photovoltaic materials we also evaluate the absorbing capabilities of the thin films under solar illumination, by defining an effective absorption depth that we relate to the ambipolar diffusion length.

Results

Determination of the ambipolar diffusion length using a laser-induced steady-state photocarrier grating. We have used the SSPG technique to characterize six different types of photovoltaic absorber materials, i.e. a-Si:H a-SiGe:H, μc-Si:H, $Cu(In,Ga)Se_2$, methylammonium lead bromide ($MAPbBr_3$) and methylammonium lead iodide-chloride ($MAPbI_{3-x}Cl_x$) perovskites. The fabrication details and references to the performance of the films in devices are found in the methods section. The films are illuminated by two laser beams, one of which passes through a chopper and another that functions as a bias beam that originates from the same laser source. When the two beams have the same polarization, they interfere to form a grating with fringes that are parallel to the electrodes. By changing the angle θ between the two laser beams, the period of the grating Λ can be altered according to the relation $\Lambda = \lambda/$

$[2\sin(\theta/2)]$, where λ is the wavelength of the laser light. The photoconductivity that is generated by the chopped laser beam is measured using two electrodes, a lock-in amplifier and a voltage source. For the measurement of the diffusion length it is not required to know the absolute value of the conductivity, as the measurement is compared to the condition in which the two laser beams have orthogonal polarization and no grating is formed. This is achieved by a half-wave plate that rotates the polarization of the bias beam perpendicular to that of the chopped beam. Provided that the intensity of the chopped (I_{chopped}) beam is much weaker than that of the bias beam (I_{bias}), the ratio of the conductivity under coherent conditions to that under incoherent conditions is written as[11]

$$\beta[\Lambda] = \frac{\sigma_{\parallel}}{\sigma_{\perp}} = 1 - \frac{2\gamma\gamma_0^2}{[1+(2\pi L_{\mathrm{d}}/\Lambda)^2]^2} \quad (1)$$

The parameter γ (with a value between 0.5 and 1) describes the dependency between the photoconductivity (σ_{ph}) and the generation rate G as $\sigma_{\mathrm{ph}} \propto G^{\gamma}$ and is measured separately by varying I_{chopped} without the presence of the bias beam. γ_0 is a grating quality factor between 0 and 1 that contains information about imperfections of the grating due to low photosensitivity of the film, mechanical vibrations, non-ideal polarization of the laser light, or scattering on the surface or in the bulk of the sample. Equation (1) can be rewritten in the more convenient form of[13]

$$[2/(1-\beta)]^{1/2} = [\Lambda^{-2}(2\pi L_{\mathrm{d}})^2 + 1]/\left[\gamma^{1/2}\gamma_0\right], \quad (2)$$

which shows that $[2/(1-\beta)]^{1/2}$ is a linear function of Λ^{-2} with a slope that is proportional to the square of the ambipolar diffusion length. Further details are given in the methods section.

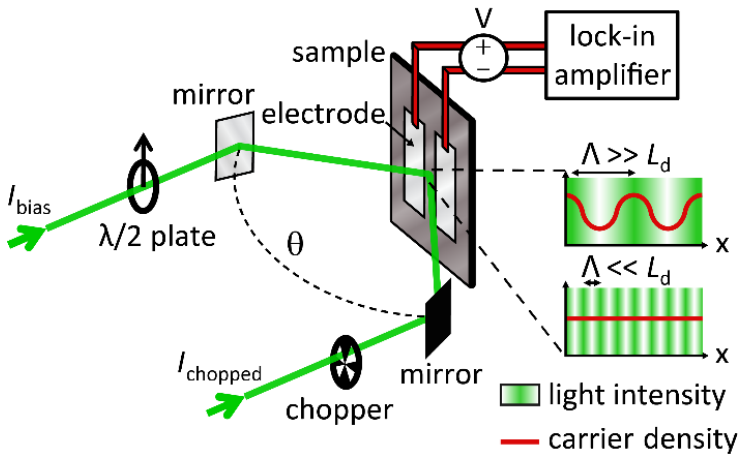

Figure 1 | Schematic of the SSPG laser grating technique. Two coherent laser beams form a laser grating, the period of which (Λ) can be controlled by changing the angle between the two beams. If Λ is much larger than the ambipolar diffusion length L_d, the generated photocarriers will be unable to diffuse across the dark fringes before recombining, which results in a reduced conductivity perpendicular to the fringes. When Λ is much smaller than L_d, the measured conductivity will be unaffected by the presence of laser grating. The ambipolar diffusion length can be found by monitoring the photoconductivity for a range of grating periods.

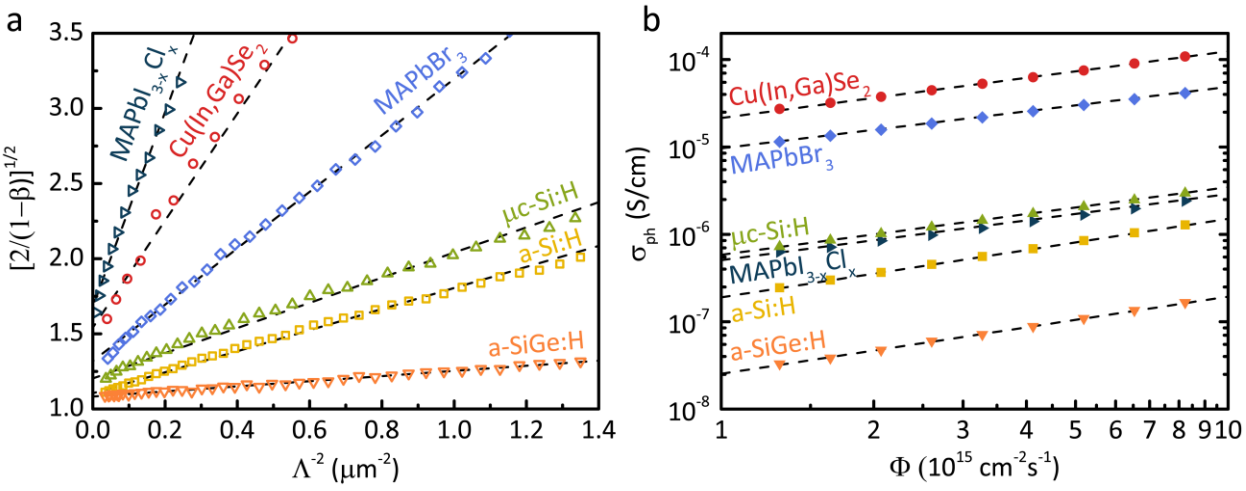

Figure 2 | Results of the SSPG measurements on a broad selection of photoactive absorber materials. a) The conductivity ratio and grating period are plotted in a linear manner; a steeper slope corresponds to a higher ambipolar diffusion length. The dashed lines are linear fits of equation (2) to the data. b) The measured photoconductivity as a function of the photon flux, plotted on a double logarithmic scale. The fitted dashed lines reveal a power law behavior from which the parameter γ is extracted.

Fig. 2 shows the linearized relation between the conductivity of the various films versus the laser grating period and the relation between photoconductivity and the photon flux. The quantities L_d and γ_0 that have been derived by fitting equation (2) to this data are shown in Table 1, together with the separately determined values of γ. The diffusion length measurements are combined with steady-state photoconductivity measurements to calculate the products of the low-field mobility μ^0 and recombination lifetime τ^R of both the minority and majority charge carriers ($\mu^0_{\mathrm{min}}\tau^{\mathrm{R}}_{\mathrm{min}}$and $\mu^0_{\mathrm{maj}}\tau^{\mathrm{R}}_{\mathrm{maj}}$) under the same measurement conditions (see methods). This method does not identify either electrons or holes as the majority carriers, but by other methods it has been found that electrons are the majority carriers for a-Si:H[14] and µc-Si:H[15], whereas holes were found to be the majority carriers for Cu(In,Ga)Se_2[16,17] and $MAPbBr_3$[18]. The difference between the minority and majority mobility-lifetime products is small for both the a-SiGe:H and $MAPbI_{3-x}Cl_x$ film, which underlines the ambipolar nature of these materials[19-21].

Table 1 | Derived parameters from the SSPG and photoconductivity measurements. The diffusion length L_d and grating quality factor γ_0 are directly extracted from the SSPG measurements. The parameter γ is obtained by intensity dependent conductivity measurements and the mobility-lifetime products are obtained by combining the SSPG measurements with photoconductivity measurements under the same illumination conditions.

Absorber material	L_d (nm)	γ_0	γ	$\mu^0_{min}\tau^R_{min}$ (cm^2V^{-1})	$\mu^0_{maj}\tau^R_{maj}$ (cm^2V^{-1})
a-SiGe:H	62 ± 3	1.00	0.87	$1.1 \pm 0.2 \times 10^{-9}$	$2.7 \pm 0.4 \times 10^{-9}$
a-Si:H	129 ± 6	0.99	0.90	$3.5 \pm 0.3 \times 10^{-9}$	$1.1 \pm 0.1 \times 10^{-7}$
μc-Si:H	145 ± 7	1.00	0.77	$4.7 \pm 0.5 \times 10^{-9}$	$3.1 \pm 0.3 \times 10^{-7}$
$Cu(In,Ga)Se_2$	288 ± 32	0.88	0.76	$1.9 \pm 0.4 \times 10^{-8}$	$9.3 \pm 0.8 \times 10^{-7}$
$MAPbBr_3$	201 ± 8	0.96	0.70	$9.4 \pm 0.8 \times 10^{-9}$	$9.8 \pm 0.8 \times 10^{-7}$
$MAPbI_{3-x}Cl_x$	367 ± 39	0.74	0.76	$5.0 \pm 3.1 \times 10^{-8}$	$7.6 \pm 3.5 \times 10^{-8}$

The fits to the measurements show a reasonable to excellent value of γ_0, underlining the high quality of the optical grating in the films and the suitability of the technique to characterize the selection of materials. For the three silicon-based materials, the diffusion length values are in agreement with previous work[12,20,22,23].

There are only a few reported diffusion lengths for $Cu(In,Ga)Se_2$ samples[24-26], with widely varying results. This is due the different composition of the materials studied and the use of different measurement conditions and analysis methods. This complicates a direct comparison of the measured value of 288 nm for the present $Cu(In.Ga)Se_2$ sample with earlier results. Here, we contribute by consistently comparing the performance of state-of-the-art $(Cu,In)GaSe_2$ with other photovoltaic absorber materials.

$MAPbI_{3-x}Cl_x$ possesses the highest diffusion length and minority carrier mobility-lifetime product of all the investigated materials, though its majority carrier mobility-lifetime product is relatively low compared to that of $MAPbBr_3$. This difference could indicate that the $MAPbBr_3$ sample contains larger crystal and/or a higher crystallinity fraction[27]. Higher diffusion length values can be found in the literature for both $MAPbBr_3$ and $MAPbI_{3-x}Cl_x$ materials, but these measurements were done in nonsteady-state conditions,

147 i.e., by photoluminescence decay measurements[28-30]. We expect these transient techniques to be more
148 sensitive to photon-recycling effects. A more extensive overview of ambipolar diffusion length
149 measurements focusing on halide perovskites focusing on the effect of processing and aging conditions
150 will be published elsewhere[31].

151

152 **Effective absorption depth.** The above charge carrier transport properties should be seen in relation to
153 the absorption capability of the films. To that end, we define an effective absorption depth for the
154 semiconductor films studies. To establish this figure of merit, we assume perfect incoupling of AM1.5G
155 radiation and a single pass through the film that absorbs according to Beer-Lambert behavior. If we
156 further assume that all absorbed photons result in collectable charge carriers we can define a
157 hypothetical optical current density J_{opt} as function of the layer thickness z:

158 $$J_{\mathrm{opt}}[z] = e \int \Phi_{\mathrm{AM1.5G}}[E][1 - \exp(-\alpha[E]z)]\,\mathrm{d}E, \qquad (5)$$

159 with $\Phi_{\mathrm{AM1.5G}}[E]$ the photon flux and $\alpha[E]$ the measured absorption coefficients, both as a function of

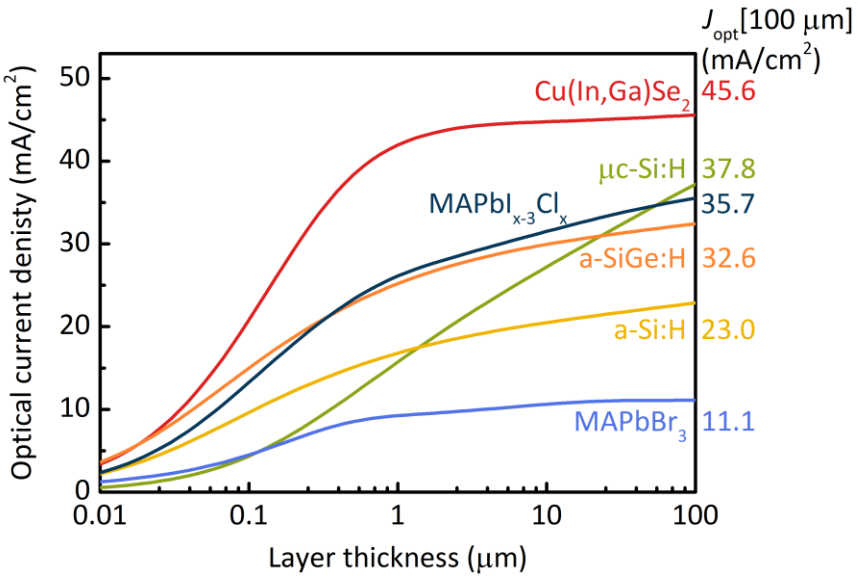

160 the photon energy E. Fig. 3 shows the optical current density as a function of the layer thickness for the

Figure 3 | Optical current density versus layer thickness for several thin film absorber materials as a function of the material thickness. The displayed optical current densities at a layer thickness of 100 µm are here defined as the maximum collectable current densities for the different absorber materials. Note that the horizontal axis has a logarithmic scale.

materials that we studied. Most of the materials show a distinct curvature after which J_{opt} saturates due to exhaustion of available photons with energies higher than the band gap. The values calculated for µc-Si:H exhibit a weak absorption considering its low band gap of ~1.1 eV, which is explained by the indirect nature of its band gap.

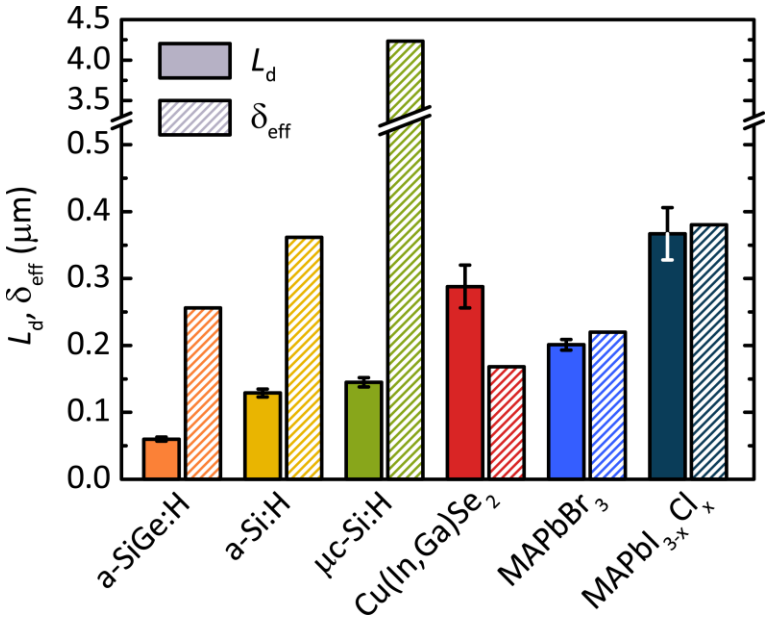

Figure 4 | Comparison between the measured ambipolar diffusion lengths and the calculated effective absorption depth. A large diffusion length L_d compared to the effective absorption depth δ_{eff} is desirable. Cu(In,Ga)Se_2, $MAPbBr_3$ and $MAPbI_{3-x}Cl_x$ perform significantly better than the three silicon based thin-film materials.

We continue by specifying a hypothetical maximum attainable current density for each material by calculating the optical current density at a layer thickness of 100 μm, $J_{\mathrm{opt}}[100\ \mu\mathrm{m}]$, which is much larger than the typical thickness of an absorber material in a thin film device. The advantage of this method is that it takes into account the absolute values of $\alpha[E]$, including those near and just below the band gap energy. This contribution to the absorption would not be taken into account if the maximum current density were calculated by summing up all photons with an energy higher than that of the band gap, as is often done, such as in the detailed balance model of Shockley-Queisser[32]. As a figure of merit for the absorbing capacity of a material we define an effective absorption depth δ_{eff} as the depth of an absorber that is required to absorb all but $1/e$ of $J_{\mathrm{opt}}[100\ \mu\mathrm{m}]$. Note that this definition is analogous to the manner in which the conventional absorption depth is defined as $1/\alpha$ for a particular photon energy.

Fig. 4 compares the ambipolar diffusion lengths and the effective absorption depths for the studied materials. For efficient current generation and collection, it is beneficial for an absorber to have a diffusion length that is much larger than its effective absorption depth. A large $L_d/\delta_{\mathrm{eff}}$ will be beneficial to the fill factor. Only for Cu(In,Ga)Se_2, $MAPbBr_3$, and $MAPbI_{3-x}Cl_x$ the diffusion length is greater than or close to the effective absorption depth. Other materials will require more rigorous internal or external light trapping schemes and/or band edge profiling engineering to compensate for this handicap. The thin-film silicon-based materials have the lowest quality within the materials set studied, although it should be noted that these materials have a higher index of refraction which amplifies the possibilities for internal light trapping[33]. For μc-Si:H, the discrepancy of the diffusion length and effective absorption depth is exceptionally large, even though the diffusion properties for this material are reported to be better in the direction of film-growth due to the preferred orientation of the crystallites[34]. The Cu(In,Ga)Se_2 film can possibly benefit as well from improved transport in the direction of film-growth due to the shape of its crystallites.

Discussion

When assessing the quality of a photovoltaic absorber material one should, apart from the photoabsorption and carrier transport properties, which affect the short circuit current (J_{sc}) and the fill factor (FF), also consider other properties, such as the difference between the value of the band gap and the attainable open circuit voltage in a device. In this respect, the lead iodide chloride perovskite absorber layer (with a voltage deficit, $\Delta V \sim 0.4$ V)[35] outperforms the other studied materials ($\Delta V \sim 0.4$-0.6 V for Cu(In,Ga)Se_2[36], $\Delta V \sim 0.6$ V for µc-Si:H[37], $\Delta V \sim 0.7$ V for $MAPbBr_3$[38], and $\Delta V \sim 0.8$-0.9 V for a-Si(Ge):H[37]).

We have shown that the steady-state photocarrier technique can be applied in a comparative way to a broad selection of photovoltaic absorber materials provided that the laser wavelength is chosen such that the light penetrates into the bulk and the incident photon flux is kept equal. The selection of materials includes copper indium gallium selenide chalcopyrite and two types of hybrid organic-inorganic lead halide perovskites, which have thus far not been compared using a single diffusion length measurement technique. The obtained ambipolar diffusion lengths are put into photovoltaic perspective by comparing them to an effective absorption depth for the solar spectrum. We observe a division between the weakly performing thin-film silicon based materials on one side and the stronger performing chalcopyrite and perovskite films on the other side, which is also resembled in the reported energy conversion efficiencies of these materials. The method that we use provides a quick but comprehensive way to assess the photovoltaic quality of a wide variety of thin film absorber layers without the need of creating and testing the materials in a full device.

Acknowledgments

The authors would like to thank Sarah Brittman for her help with the fabrication of the perovskite films and her valuable discussions that contributed to this work. L.W. Veldhuizen and R.E.I. Schropp acknowledge the support NanoNextNL (project 02A.03), a micro and nanotechnology consortium of the government of the Netherlands and 130 partners. G.W.P. Adhyaksa, and E.C. Garnett acknowledge financial support from the European Research Council under the European Union's Seventh Framework Programme (FP/2007-2013)/ERC Grant Agreement no. 337328, "NanoEnabledPV," and from an industrial partnership between Philips and FOM.

Methods

Preparation of the absorber materials. The a-Si:H, a-SiGe:H and μc-Si:H samples in this study were grown on Corning EAGLE XG® glass using hot wire chemical vapor deposition with SiH_4, GeH_4, and H_2 as source gasses. Pure a-Si:H has an optical band gap of 1.84 eV. The a-SiGe:H layer has a germanium content of 45% and an optical band gap of 1.54 eV. Both the a-Si:H and a-SiGe:H films have a thickness of ~200 nm whereas the μc-Si:H film was made to have a thickness of ~1μm due to its lower absorption coefficients at the relevant wavelengths. In order to fabricate the μc-Si:H film, a SiH_4/H_2 source gas ratio of 0.05 was used which resulted in a film with a Raman crystallinity of 65% . The samples were light-soaked for multiple hours before the measurement. A description of the deposition setup as well as a more detailed description of the material properties can be found in previous publications[39,40].

For the preparation of the $Cu(In,Ga)Se_2$ sample, molybdenum films were deposited on soda-lime glass by DC magnetron sputtering. Subsequently, a ~2 μm $Cu(In,Ga)Se_2$ film was deposited by a coevaporation bithermal (380°C-580°C) three-stage process[41,42]. Growing the films this way ensures a standard sodium diffusion leading to device-grade material[41,43], but hinders a successful SSPG measurements because of the highly conductive molybdenum layer. The molybdenum layer was therefore removed using a lift-off

process by gluing soda lime glass on top of the sample using EPO-TEK 353 ND glue and subsequent mechanical separation[42]. This process provides a $Cu(In,Ga)Se_2$ film with the exact composition and structure as in a solar cell, but on an insulating substrate and with a smooth film/air interface that can be easily probed with the SSPG measurement. Note that for the SSPG measurement the sample is illuminated from the substrate side of the thin film in the commonly used solar cell configuration.

For the mixed halide perovskite samples, soda-lime glass substrates were cleaned using acetone(15 min), isopropanol (15 min) and hydrochloric acid (18 % in deionized water, for 1-2 hours) . To make a hydrophilic surface, the substrates were treated with an oxygen plasma (50 W, 2 min) immediately before perovskite deposition. The perovskite films were made in a glovebox by spin-coating a 2M perovskite solution in DMF for $MAPbBr_3$ and 1M perovskite solution in DMSO for $MAPbI_{3-x}Cl_3$ for 60 seconds at 10,000 rpm and a subsequent 30 minute annealing treatment at 100°C. The perovskite solutions were synthesized by mixing methylammonium halides (CH_3NH_3X) and lead halide (PbX_2) precursors with equimolar concentrations. Here, X represents the halide, which is bromide for the $MAPbBr_3$ film (with an optical bandgap of 2.24 eV) and iodine and chlorine in a ratio of 3:1 for the $MAPbI_{3-x}Cl_x$ film (with an optical band gap of 1.55 eV). The layers have a thickness of ~300 nm. Further details can be found in previous reports[31,44]

Steady-state photocarrier grating technique. For the ambipolar diffusion length measurements with the SSPG technique, two coplanar Au (for the perovskite films) or Ag (for the other films) strip electrodes with a spacing of 0.6 mm are evaporated on our photoactive films. It has been verified with a linearity *IV* test that these electrodes provide a low Ohmic contact to all semiconductor films studied. We have used 532 nm laser light for all samples except for the $Cu(In,Ga)Se_2$ film where a 633 nm laser light was required in order to achieve a more homogeneous light intensity throughout the sample depth. Both lasers were calibrated to have a photon flux of 5×10^{16} $cm^{-2}s^{-1}$ measured at the sample position, leading

to volume-averaged generation rates of G = 10^{20}-10^{21} $cm^{-3}s^{-1}$ for the studied samples. The laser beam is guided through a linear polarization filter that controls the laser beam intensity in combination with an automated rotatable half-wave plate to measure the power dependency (γ) between the photoconductivity and the generation rate. Via this way the photon flux can be varied between 10^{15} and 10^{16} $cm^{-2}s^{-1}$. The conductivities are measured with a lock-in amplifier (SR510) under a small applied electric field strengths of E = 20-200 V/cm for which we made sure that the diffusion lengths are independent of the field intensity and thus fulfill the condition for ambipolar transport. Besides the influence of the electric field strength E, we have also investigated the dependency of the photon flux Φ and the chopper frequency on the value of L_d (see Supplementary Information Fig. S1)

The minority and majority carrier mobility-lifetime products are calculated by solving the pair of equations[45]

$$L_{\mathrm{d}}^2 = [\gamma + 1]\frac{kT}{e}\frac{\mu_{\mathrm{min}}^0 \tau_{\mathrm{min}}^{\mathrm{R}} \mu_{\mathrm{maj}}^0 \tau_{\mathrm{maj}}^{\mathrm{R}}}{\mu_{\mathrm{min}}^0 \tau_{\mathrm{min}}^{\mathrm{R}} + \mu_{\mathrm{maj}}^0 \tau_{\mathrm{maj}}^{\mathrm{R}}} \quad (3)$$

and

$$\sigma_{\mathrm{ph}} = eG\left[\mu_{\mathrm{min}}^0 \tau_{\mathrm{min}}^{\mathrm{R}} + \mu_{\mathrm{maj}}^0 \tau_{\mathrm{maj}}^{\mathrm{R}}\right], \quad (4)$$

where e is the elementary charge and G is the average volume generation rate. The photoconductivity is measured at the same laser wavelength, photon flux, and voltage as the diffusion length measurements.

Uncertainties. The fitting standard errors are smaller than 2% for all diffusion length measurements. The uncertainties of the derived ambipolar diffusion lengths are therefore not based on the quality of the fits but on the uncertainty of θ, which is the dominant contributor to the uncertainty of L_d. We estimate the uncertainty of θ to be 1° due to possible laser and sample misalignments. In order to resolve the longer diffusion length of the $Cu(In,Ga)Se_2$ and $MAPbI_{3-x}Cl_x$ absorbers, θ values smaller than 5° were

required. This is the reason that the diffusion length of these materials have a higher uncertainty than that of the other measured absorber materials (Table 1). The uncertainties of L_d, together with uncertainties of the photon flux (~10%) are propagated to obtain the errors of the mobility-lifetime products.

Optical constants The optical constants that were used to calculate the optical current densities were obtained by spectral ellipsometry and reflection-transmission measurements.

References

1 Hodes, G. & Kamat, P. V. Understanding the Implication of Carrier Diffusion Length in Photovoltaic Cells. *The journal of physical chemistry letters* **6**, 4090-4092, doi:10.1021/acs.jpclett.5b02052 (2015).

2 Faughnan, B., Moore, A. & Crandall, R. Relationship between collection length and diffusion length in amorphous silicon. *Applied Physics Letters* **44**, 613-615, doi:10.1063/1.94852 (1984).

3 Faughnan, B. W. & Crandall, R. S. Determination of carrier collection length and prediction of fill factor in amorphous silicon solar cells. *Applied Physics Letters* **44**, 537-539, doi:10.1063/1.94830 (1984).

4 Beck, N., Wyrsch, N., Hof, C. & Shah, A. Mobility lifetime product—A tool for correlating a-Si:H film properties and solar cell performances. *Journal of Applied Physics* **79**, 9361-9368, doi:10.1063/1.362614 (1996).

5 Khanna, V. K. Physical understanding and technological control of carrier lifetimes in semiconductor materials and devices: A critique of conceptual development, state of the art and applications. *Progress in Quantum Electronics* **29**, 59-163, doi:10.1016/j.pquantelec.2005.01.002 (2005).

6 Spear, W. E. Drift mobility techniques for the study of electrical transport properties in insulating solids. *Journal of Non-Crystalline Solids* **1**, 197-214, doi:10.1016/0022-3093(69)90001-5 (1969).

7 Ahrenkiel, R. K. Measurement of minority-carrier lifetime by time-resolved photoluminescence. *Solid-State Electronics* **35**, 239-250, doi:10.1016/0038-1101(92)90228-5 (1992).

8 Dexheimer, S. L. *Terahertz Spectroscopy*. (CRC Press, 2007).

9 Kronik, L. Surface photovoltage phenomena: theory, experiment, and applications. *Surface Science Reports* **37**, 1-206, doi:10.1016/s0167-5729(99)00002-3 (1999).

10 Shah, A. V., Sauvain, E. & Hubin, J. Characteristic lengths for transport in illuminated intrinsic a-Si:H. *Journal of Non-Crystalline Solids* **114**, 402-404, doi:10.1016/0022-3093(89)90598-x (1989).

11 Ritter, D., Zeldov, E. & Weiser, K. Steady-state photocarrier grating technique for diffusion length measurement in photoconductive insulators. *Applied Physics Letters* **49**, 791-793, doi:10.1063/1.97548 (1986).

12 Brüggemann, R. Steady-state photocarrier grating technique for the minority-carrier characterisation of thin-film semiconductors. *Journal of Physics: Conference Series* **253**, 012081, doi:10.1088/1742-6596/253/1/012081 (2010).

13 Balberg, I., Delahoy, A. E. & Weakliem, H. A. Self-consistency and self-sufficiency of the photocarrier grating technique. *Applied Physics Letters* **53**, 992-994, doi:10.1063/1.100051 (1988).

14 Street, R. A. *Hydrogenated Amorphous Silicon*. (Cambridge University Press, 1991).

15 Wang, F., Liu, H. N., He, Y. L., Schweiger, A. & Schwarz, R. Transient and steady-state optoelectronic properties of μc-Si:H. *Journal of Non-Crystalline Solids* **137-138**, 511-514, doi:10.1016/s0022-3093(05)80167-x (1991).

16 Scheer, R. & Schock, H.-W. *Chalcogenide Photovoltaics*. 262 (Wiley-VCH, 2011).

17 Dymshits, A., Rotem, A. & Etgar, L. High voltage in hole conductor free organo metal halide perovskite solar cells. *J. Mater. Chem. A* **2**, 20776-20781, doi:10.1039/c4ta05613b (2014).

18 Kedem, N. *et al.* Light-Induced Increase of Electron Diffusion Length in a p-n Junction Type CH3NH3PbBr3 Perovskite Solar Cell. *The journal of physical chemistry letters* **6**, 2469-2476, doi:10.1021/acs.jpclett.5b00889 (2015).

19 Li, F. *et al.* Ambipolar solution-processed hybrid perovskite phototransistors. *Nature communications* **6**, 8238, doi:10.1038/ncomms9238 (2015).

20 Wickboldt, P. *et al.* Ambipolar Phototransport ($\mu\tau_e = \mu\tau_h$) Observed as an Intrinsic Property of a-SiGe:H. *MRS Proceedings* **467**, 263-268, doi:10.1557/proc-467-263 (1997).

21 Hsieh, S. W. *et al.* Ambipolar Performances of Novel Amorphous Silicon-Germanium Alloy Thin-Film Transistors. *Japanese Journal of Applied Physics* **32**, L1043-L1045, doi:10.1143/jjap.32.l1043 (1993).

22 Hegedus, S. S. Current–Voltage Analysis of a-Si and a-SiGe Solar Cells Including Voltage-dependent Photocurrent Collection. *Progress in Photovoltaics: Research and Applications* **5**, 151-168, doi:10.1002/(sici)1099-159x(199705/06)5:3<151::aid-pip167>3.0.co;2-w (1997).

23 Brüggemann, R., Badran, R. I. & Xiong, S. Relation between the dark and photoelectronic properties of microcrystalline silicon. *Journal of Optoelectronics and Advanced Materials* **9**, 348-351 (2007).

24 Zweigart, S., Menner, R., Klenk, R. & Schock, H. W. Application of Steady-State Photocarrier Grating Technique for Determination of Ambipolar Diffusion Lengths in Cu(In, Ga)(S, $Se)_2$-Thin Films for Solar Cells. *Materials Science Forum* **173-174**, 337-342, doi:10.4028/www.scientific.net/MSF.173-174.337 (1995).

25 Brown, G. *et al.* Determination of the minority carrier diffusion length in compositionally graded Cu(In,Ga)Se[sub 2] solar cells using electron beam induced current. *Applied Physics Letters* **96**, 022104, doi:10.1063/1.3291046 (2010).

26 Dinca, S. A. *et al.* Electron drift-mobility measurements in polycrystalline CuIn1−xGaxSe2 solar cells. *Applied Physics Letters* **100**, 103901, doi:10.1063/1.3692165 (2012).

27 Choi, J. J., Yang, X., Norman, Z. M., Billinge, S. J. & Owen, J. S. Structure of methylammonium lead iodide within mesoporous titanium dioxide: active material in high-performance perovskite solar cells. *Nano letters* **14**, 127-133, doi:10.1021/nl403514x (2014).

28 Sheng, R. *et al.* Methylammonium Lead Bromide Perovskite-Based Solar Cells by Vapor-Assisted Deposition. *The Journal of Physical Chemistry C* **119**, 3545-3549, doi:10.1021/jp512936z (2015).

29 Stranks, S. D. *et al.* Electron-hole diffusion lengths exceeding 1 micrometer in an organometal trihalide perovskite absorber. *Science* **342**, 341-344, doi:10.1126/science.1243982 (2013).

30 Wehrenfennig, C., Eperon, G. E., Johnston, M. B., Snaith, H. J. & Herz, L. M. High Charge Carrier Mobilities and Lifetimes in Organolead Trihalide Perovskites. *Advanced Materials* **26**, 1584-1589, doi:10.1002/adma.201305172 (2014).

31 Adhyaksa, G. W. P. *et al.* Diffusion lengths in hybrid perovskites: processing, composition, aging and surface passivation effects. *sumbitted to Chemistry of Materials*.

32 Shockley, W. & Queisser, H. J. Detailed Balance Limit of Efficiency of p-n Junction Solar Cells. *Journal of Applied Physics* **32**, 510-519, doi:10.1063/1.1736034 (1961).

33 Tiedje, T., Yablonovitch, E., Cody, G. D. & Brooks, B. G. Limiting efficiency of silicon solar cells. *IEEE Transactions on Electron Devices* **31**, 711-716, doi:10.1109/t-ed.1984.21594 (1984).

34 Švrček, V. *et al.* Transport anisotropy in microcrystalline silicon studied by measurement of ambipolar diffusion length. *Journal of Applied Physics* **89**, 1800-1805, doi:10.1063/1.1338996 (2001).

35 Jeon, N. J. *et al.* Compositional engineering of perovskite materials for high-performance solar cells. *Nature* **517**, 476-480, doi:10.1038/nature14133 (2015).

36 Jackson, P. *et al.* Cover Picture: Properties of Cu(In,Ga)Se2solar cells with new record efficiencies up to 21.7% (Phys. Status Solidi RRL 1/2015). *physica status solidi (RRL) - Rapid Research Letters* **9**, n/a-n/a, doi:10.1002/pssr.201570601 (2015).

37 Yan, B., Yang, J. & Guha, S. Amorphous and nanocrystalline silicon thin film photovoltaic technology on flexible substrates. *Journal of Vacuum Science & Technology A: Vacuum, Surfaces, and Films* **30**, 04D108, doi:10.1116/1.4707154 (2012).

38 Heo, J. H., Song, D. H. & Im, S. H. Planar $CH_3NH_3PbBr_3$ hybrid solar cells with 10.4% power conversion efficiency, fabricated by controlled crystallization in the spin-coating process. *Advanced Materials* **26**, 8179-8183, doi:10.1002/adma.201403140 (2014).

39 Veldhuizen, L. W. *et al.* Optimization of hydrogenated amorphous silicon germanium thin films and solar cells deposited by hot wire chemical vapor deposition. *Thin Solid Films* **595**, 226-230, doi:10.1016/j.tsf.2015.05.055 (2015).

40 van Veen, M. K. & Schropp, R. E. I. Amorphous silicon deposited by hot-wire CVD for application in dual junction solar cells. *Thin Solid Films* **403-404**, 135-138, doi:10.1016/s0040-6090(01)01642-x (2002).

41 Couzinié-Devy, F., Barreau, N. & Kessler, J. Re-investigation of preferential orientation of Cu(In,Ga)Se2 thin films grown by the three-stage process. *Progress in Photovoltaics: Research and Applications* **19**, 527-536, doi:10.1002/pip.1079 (2011).

42 Harel, S., Tomassini, M., Arzel, L., Gautron, E. & Barreau, N. Impact of Mo density on Mo/CIGSe interfaces: An XPS study. 0425-0430, doi:10.1109/pvsc.2014.6924950 (2014).

43 Theelen, M. *et al.* The impact of atmospheric species on the degradation of CIGS solar cells. *Solar Energy Materials and Solar Cells* **141**, 49-56, doi:10.1016/j.solmat.2015.05.019 (2015).

44 Noh, J. H., Im, S. H., Heo, J. H., Mandal, T. N. & Seok, S. I. Chemical management for colorful, efficient, and stable inorganic-organic hybrid nanostructured solar cells. *Nano letters* **13**, 1764−1769, doi:10.1021/nl400349b (2013).

45 Shah, A., Sauvajn, E., Hubin, J., Pipoz, P. & Hof, C. Free carrier ambipolar diffusion length in amorphous semiconductors. *Philosophical Magazine Part B* **75**, 925-936, doi:10.1080/13642819708205717 (1997).

Supplementary information

To test the sensitivity of the SSPG method as used for the determination of the ambipolar diffusion length to experimental parameters, we varied the illumination intensity (photon flux), electric field (voltage between the contacts) and the chopper frequency. Here we present the relative changes in L_d for two materials from the set of materials studied with significantly different dielectric constants, a-Si:H and $MAPbBr_3$.

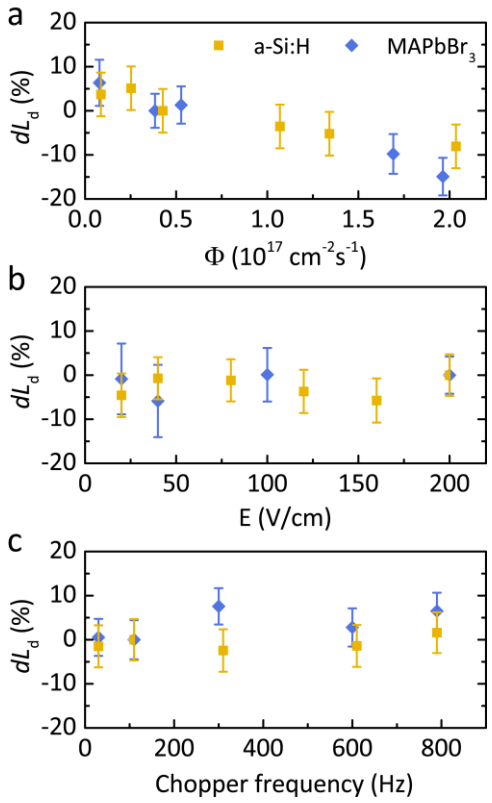

Figure S1 | The relative change in the ambipolar diffusion length dL_d of a-Si:H and $MAPbBr_3$ as a fucntion of several measurement conditions. a) The effect of the total photon flux Φ of the laser beams (chopped and bias beam). For both materials, L_d is seen to decrease with increasing photon flux. This can explaned by the increased quasi-Fermi level splitting at higher illumination intensities, causing an increase in the number of recombination centers and a reduction of the recombination lifetime τ^R. b) The effect of the electric field strength E. No significant influence is observed, confirming that the

measurements are performed under conditions for ambipolar transport. c) The influence of the chopper frequency. The diffusion length stays within the error bars for all investigated frequencies. This is ensures that the measurements are performed outside the regime of dielectric relaxation.